AGU PUBLICATIONS

Water Resources Research

RESEARCH ARTICLE
10.1002/2015WR017552

Linking water age and solute dynamics in streamflow at the Hubbard Brook Experimental Forest, NH, USA

Paolo Benettin[1], Scott W. Bailey[2], John L. Campbell[2], Mark B. Green[2,3], Andrea Rinaldo[1,4], Gene E. Likens[5,6], Kevin J. McGuire[7], and Gianluca Botter[4]

[1]Laboratory of Ecohydrology ECHO/IIE/ENAC, École Polytechinque Fédérale de Lausanne, Lausanne, Switzerland, [2]U.S. Forest Service Northern Research Station, Hubbard Brook Experimental Forest, North Woodstock, New Hampshire, USA, [3]Center for the Environment, Plymouth State University, Plymouth, New Hampshire, USA, [4]Dipartimento ICEA, Università degli studi di Padova, Padua, Italy, [5]Cary Institute of Ecosystem Studies, Millbrook, New York, USA, [6]Department of Ecology and Evolutionary Biology, University of Connecticut, Storrs, Connecticut, USA, [7]Virginia Water Resources Research Center, Department of Forest Resources and Environmental Conservation, Virginia Tech, Blacksburg, Virginia, USA

Abstract We combine experimental and modeling results from a headwater catchment at the Hubbard Brook Experimental Forest (HBEF), New Hampshire, USA, to explore the link between stream solute dynamics and water age. A theoretical framework based on water age dynamics, which represents a general basis for characterizing solute transport at the catchment scale, is here applied to conservative and weathering-derived solutes. Based on the available information about the hydrology of the site, an integrated transport model was developed and used to compute hydrochemical fluxes. The model was designed to reproduce the deuterium content of streamflow and allowed for the estimate of catchment water storage and dynamic travel time distributions (TTDs). The innovative contribution of this paper is the simulation of dissolved silicon and sodium concentration in streamflow, achieved by implementing first-order chemical kinetics based explicitly on dynamic TTD, thus upscaling local geochemical processes to catchment scale. Our results highlight the key role of water stored within the subsoil glacial material in both the short-term and long-term solute circulation. The travel time analysis provided an estimate of streamflow age distributions and their evolution in time related to catchment wetness conditions. The use of age information to reproduce a 14 year data set of silicon and sodium stream concentration shows that, at catchment scales, the dynamics of such geogenic solutes are mostly controlled by hydrologic drivers, which determine the contact times between the water and mineral interfaces. Justifications and limitations toward a general theory of reactive solute circulation at catchment scales are discussed.

Key Points:
- Upscaling of local geochemical processes to catchment scales
- Water stored within the subsoil glacial material is actively involved in solute circulation
- Dynamic TTDs explain the variability in stream silicon concentration

Supporting Information:
- Supporting Information S1

Correspondence to:
P. Benettin,
paolo.benettin@epfl.ch

Citation:
Benettin, P., S. W. Bailey, J. L. Campbell, M. B. Green, A. Rinaldo, G. E. Likens, K. J. McGuire, and G. Botter (2015), Linking water age and solute dynamics in streamflow at the Hubbard Brook Experimental Forest, NH, USA, *Water Resour. Res.*, *51*, 9256–9272, doi:10.1002/2015WR017552.

Received 16 MAY 2015
Accepted 4 NOV 2015
Accepted article online 6 NOV 2015
Published online 28 NOV 2015

1. Introduction

Understanding streamflow sources and their impact on river hydrochemistry is a common problem in hydrology with direct implications for the protection and management of water resources worldwide. Highly monitored watersheds hosting multidisciplinary experimental activities provide unique opportunities to investigate catchment functioning from different perspectives [*Burt*, 1994; *Lindenmayer et al.*, 2012]. The availability of extensive data sets encompassing water quantity and quality, possibly over long periods and at high frequency, is considered a necessary requirement for proper process representation [*McDonnell and Beven*, 2014]. These data sets may also trigger feedbacks with hydrologic modeling, in a setting where models can be guided by and critically compared to existing measurements to provide quantitative information on catchment functioning. Typical data sets include stream discharge and solute concentration, which are integrated measures of the heterogeneous contributions to runoff from spatially distinct sources across the catchment [e.g. *Likens*, 2013]. Such integrated measurements go along with catchment-scale modeling approaches because they integrate spatial heterogeneity and allow parsimonious model development.

The study of water age dynamics plays an important role in deciphering the processes that underly observed flow and transport attributes. Travel time distributions (TTDs) subsume catchment heterogeneity, connectivity, and its temporal variations, so they can be efficiently used to investigate the integrated water and solute response of a watershed [*McGuire and McDonnell*, 2006]. The recent availability of high-quality data sets [e.g., *Neal et al.*, 2012; *Aubert et al.*, 2013] concurrent with recent advances in the theoretical

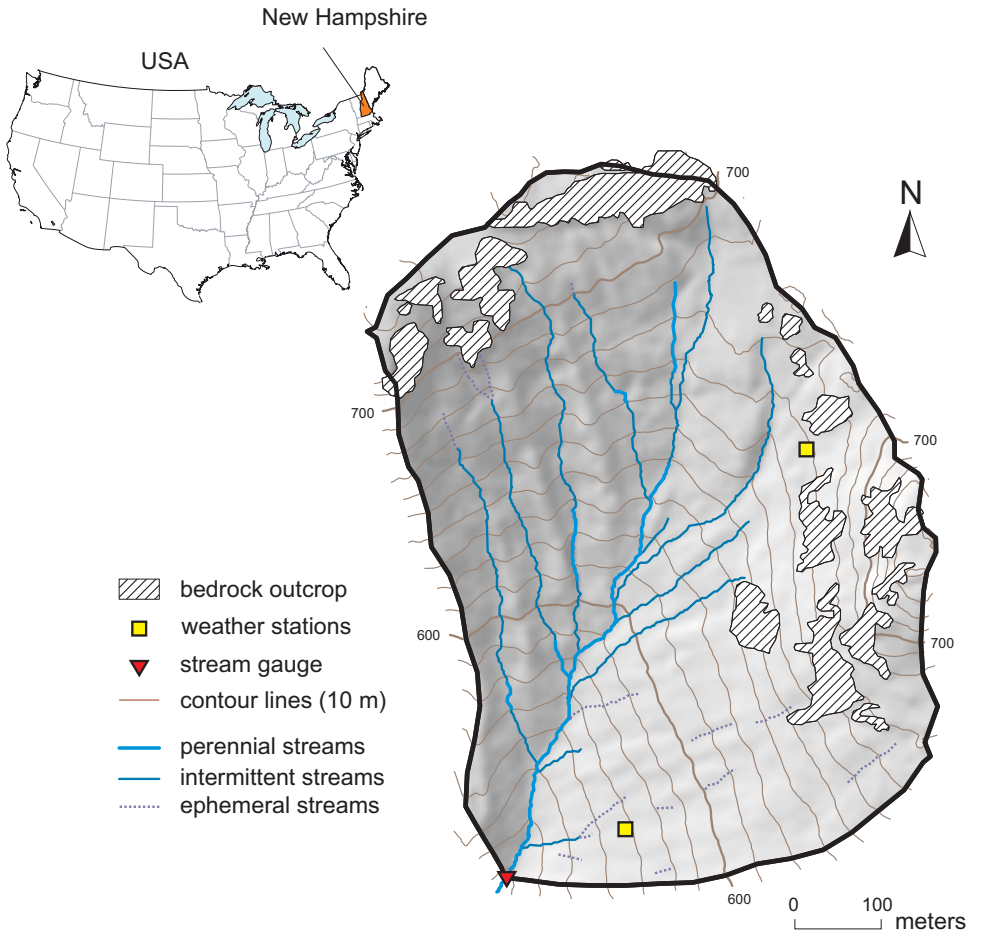

Figure 1. Map of WS3 (0.42 km^2). Elevation is expressed in m asl.

description of transport processes [*Botter et al.*, 2010, 2011; *van der Velde et al.*, 2012; *Hrachowitz et al.*, 2013; *Harman*, 2015; *Benettin et al.*, 2015a; *Rinaldo et al.*, 2015] favored an advancement in travel time research in recent years, with application to tracer studies [*van der Velde et al.*, 2010; *Birkel et al.*, 2012; *McMillan et al.*, 2012; *Heidbuechel et al.*, 2012; *Davies et al.*, 2013; *Benettin et al.*, 2013a; *Harman and Kim*, 2014; *van der Velde et al.*, 2014; *Seeger and Weiler*, 2014; *Birkel et al.*, 2015; *Queloz et al.*, 2015; *Benettin et al.*, 2015b; *Hrachowitz et al.*, 2015]. The concept of catchment travel times often has been deemed to be fundamental for biogeochemistry [*Rinaldo and Marani*, 1987; *Kirchner et al.*, 2000; *McGuire et al.*, 2007], because the time water spends within a watershed can be considered as the time available for biogeochemical processes to occur, and it can also be seen as a surrogate for distinguishing spatial sources of runoff or the storage volume over which solutes are mixing. One noteworthy example is represented by weathering processes, with several papers relating dissolved silicon dynamics to catchment hydrologic conditions and travel times [Johnson et al., 1968, 1969, 1981; *Lawrence and Driscoll*, 1990; *Hornberger et al.*, 2001; *Scanlon et al.*, 2001; *Asano et al.*, 2003; *Stelzer and Likens*, 2006; *Godsey et al.*, 2009; *Maher*, 2010, 2011; *Clymans et al.*, 2013; *Peters et al.*, 2014]. However, no studies explicitly incorporated the variability of hydrologic conditions into time-variable TTDs and used them to drive simple first-order chemical kinetics and estimate catchment-scale solute flux, which is done in this paper.

In this study, we develop a transport model for a watershed at the Hubbard Brook Experimental Forest (HBEF), USA, that is guided by detailed knowledge of the hydropedology of the site [e.g., *Detty and McGuire*, 2010a, 2010b; *Likens*, 2013; *Bailey et al.*, 2014; *Gannon et al.*, 2014; *Gillin et al.*, 2015]. The model is calibrated against available data, including stream discharge, deuterium content, and silicon and sodium concentrations and is used to address the following research objectives: (i) combining isotope and

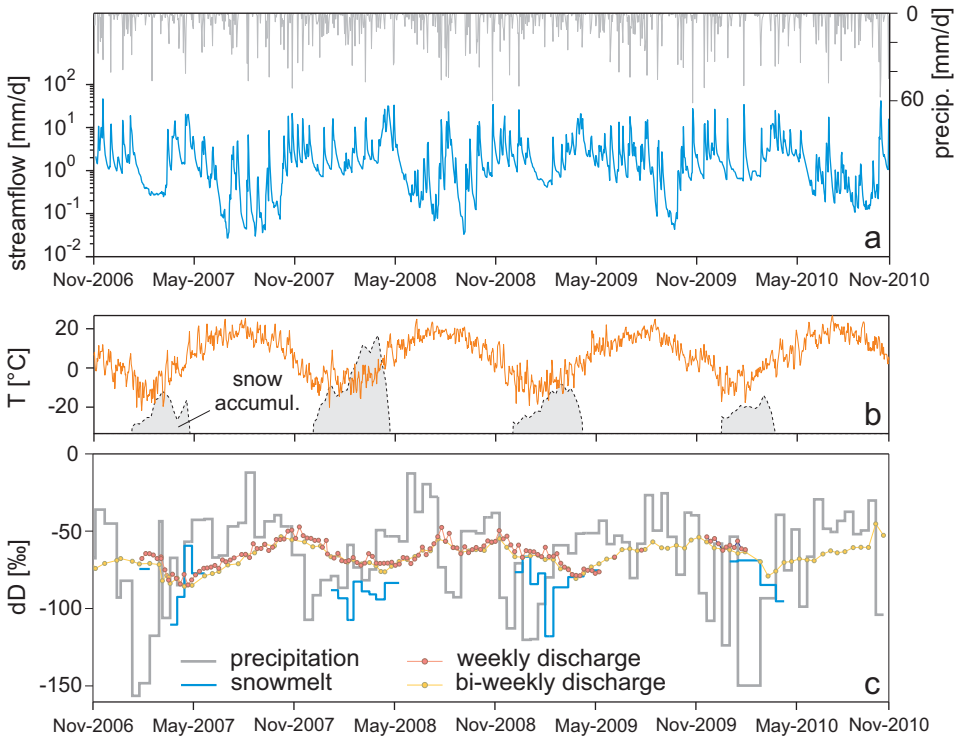

Figure 2. Measured data from November 2006 to November 2010. (a) Weather seasonality is visible in the stream discharge, where the lowest flows occur during warm summer periods and highest flows during snowmelt. (c) The deuterium content of precipitation mostly follows (b) the air temperature pattern, while the deuterium signal in the discharge is damped and shifted later by about 50 days.

hydrologic measurements to quantify the catchment-scale contribution of different runoff sources to total discharge and estimating the contributing water storage of the catchment; (ii) inferring the characteristic travel times of water through the catchment as well as their temporal dynamics; and (iii) testing the suitability of inferred travel times dynamics to quantify the release of weathering-derived solutes, namely silicon and sodium.

2. Study Area and Field Sampling

The study site is Watershed 3 (WS3, 0.42 km^2) of the HBEF, which is located within the southern White Mountains of central New Hampshire, USA (43°56′N, 71°45′W, Figure 1). Catchment-scale element budget studies were pioneered at HBEF, enabled by long-term measurement of solute fluxes into the system from atmospheric precipitation and out via streamflow. An early objective of the work was quantification of cation denudation rates and description of chemical weathering processes [Johnson et al., 1968]. WS3 is the hydrologic reference catchment for a series of long-term paired catchment studies [*McGuire and Likens*, 2011; *Likens*, 2013] and has been a center for hillslope hydrology studies [*Hooper and Shoemaker*, 1986; *Cedarholm*, 1994; *Detty and McGuire*, 2010a, 2010b; *Gannon et al.*, 2014] at HBEF.

Aerially averaged daily precipitation and continuous stream discharge records for WS3 date back to 1957. The climate is humid continental with mean monthly temperatures ranging from −9 to 18°C and annual precipitation of about 1400 mm of which a quarter to a third falls as snow [*A. S. Bailey et al.*, 2003]. Streamflow has a marked seasonality due to the snow accumulation and snowmelt cycles (Figures 2a and 2b). During dry summer periods, most of the first-order streams dry up and second-order streamflow is mostly sustained by a number of perennial seeps that are characterized by a distinctive chemical composition [*Zimmer et al.*, 2013].

Bedrock of the catchment is sillimanite-grade pelitic schist and calc-silicate granulite of the Silurian Rangeley Formation. The region was glaciated by the sequence of Pleistocene glaciations; the latest Wisconsinan glacier retreated from the HBEF area about 14,000 years ago [*Likens and Davis*, 1975] leaving basal tills and water-

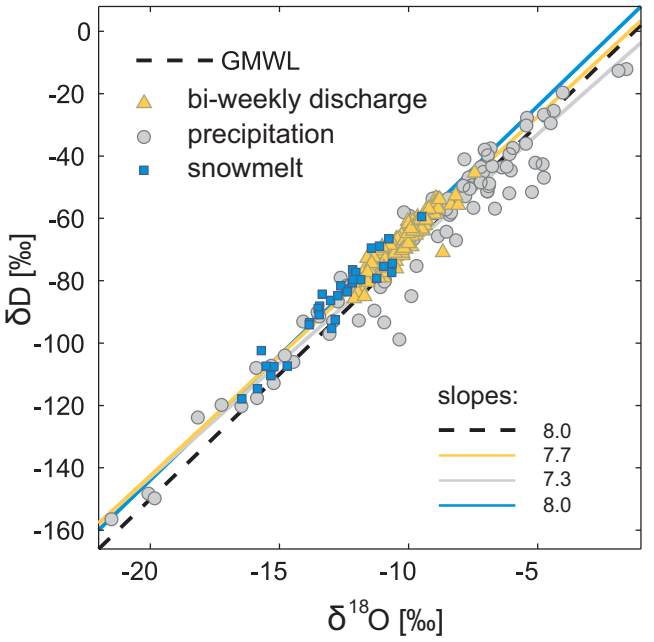

Figure 3. Water line plots for precipitation, discharge, and snowmelt samples. The plot also reports the interpolating lines compared to the Global Meteoric Water Line (GMWL), indicating no evidence of fractionation.

worked glacial drift of granitic composition and varying thickness, texture, and hydraulic conductivity [*S. Bailey et al.*, 2003, *Bailey et al.*, 2014]. Plagioclase feldspar of oligoclase composition is present in both the bedrock and glacial deposits and is likely the major source of Na^+ and H_2SiO_4 released by primary mineral weathering reactions [*S. Bailey et al.*, 2003]. *Bailey et al.* [2014] and *Gannon et al.* [2014] describe the soils as podzols with distinct variations in horizonation supporting a hydropedological functional classification with a broad range of drainage classes, soil morphology, and soil development history. The average slope in WS3 is 29% and the aspect is dominantly southern with elevation ranging from 527 to 732 m. The northern hardwood forest is dominated by *Fagus grandifolia* Ehrh. (American beech), *Acer saccharum* Marsh. (sugar maple), *Betula alleghaniensis* Britt. (yellow birch) and with *Picea rubens* Sarg. (red spruce), *Abies balsamea* (L.) Mill. (balsam fir), and *Betula papyrifera* (paper birch) in shallow-to-bedrock areas.

Water sampling for isotopic analysis occurred in WS3 from November 2006 to November 2010 (4 years total). Precipitation and snowmelt samples were collected biweekly and stream samples were collected at least weekly. Further details on isotope sampling and analyses are reported in Appendix A. Even though the sampling frequency is rather coarse relative to the timing of the hydrologic response, the almost 160 samples were collected during very different hydrologic conditions, including some high-discharge events. Deuterium in precipitation varied seasonally, with lower values in winter and higher values in summer (Figure 2c). This temporal pattern reflects the isotopic composition of the air mass source and factors that influence its moisture during atmospheric transport, such as temperature, the amount of rainout, and prevailing weather patterns [*Dansgaard*, 1964; *Gat*, 1996]. The seasonal increases in deuterium in precipitation that were observed during summer are typical of the northeastern U.S. and in part reflect atmospheric water that has been recycled/recondensed and evaporated at warm temperatures during summer [see *Ingraham*, 1998]. The amplitude of the deuterium signal is pronounced at HBEF because of snow inputs and the climate variability associated with the latitude and elevation of the site. The water stable isotopes of water reported on a meteoric water line plot (Figure 3) do not show evidence of significant fractionation, and even if some evaporative fractionation were to occur in summer, it appears negligible compared to the seasonal fluctuations of the signal and the uncertainty inherent in the data.

Other water quality measurements are available for WS3, including weekly stream water samples analyzed for silicon and sodium by inductively coupled plasma spectrometry. All of the major cations and anions have been measured in precipitation and stream water at the HBEF since 1963 [*Likens*, 2013]. Such a long-term data set provides an opportunity to investigate the hydrologic control on the release of solutes produced by mineral weathering. In this study, we focus on silicon and sodium as two solutes that are most representative of weathering processes, being little affected by soil exchange or biologic cycling. As a neutral ion, H_2SiO_4 is not subject to soil exchange processes, while Na^+, with a low charge density, is a minor component of the cation-exchange complex [*Conley et al.*, 2008; *S. Bailey et al.*, 2003; *Johnson et al.*, 1991]. Sodium, as a very minor nutrient, is little taken up by vegetation [*Subbarao et al.*, 2003; *S. Bailey et al.*, 2003]. Likewise, while silicon uptake by vegetation and storage of biogenic amorphous silicon soil pools has come

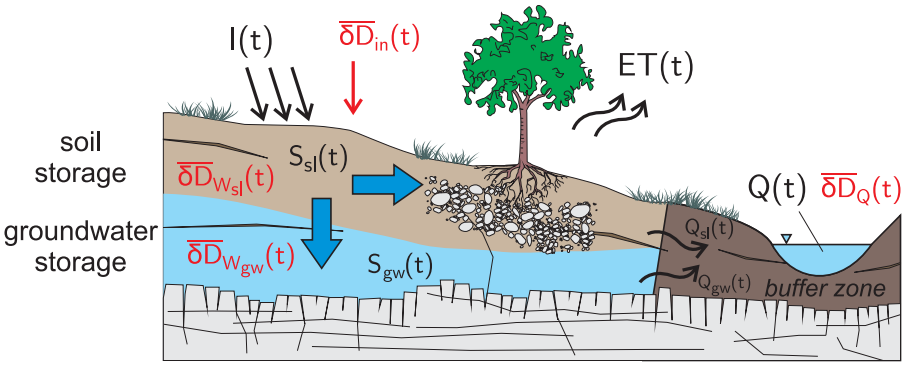

Figure 4. Illustration of the conceptual hydrochemical model, with the partitioning into soil layer, groundwater storage, and riparian buffer zone.

to be recognized [*Saccone et al.*, 2008], there is little evidence of temporal dynamics of these pools in the steady state, mature forest [*Conley et al.*, 2008], like at WS3.

3. Methods

3.1. Transport Model

The representation of an idealized hillslope soil catena presented by *Bailey et al.* [2014] provides a framework to conceptualize the catchment as three interconnected hydrologic compartments (Figure 4): soil storage, which is meant to represent the soil layers from the topsoil to the upper drift material (i.e., O to upper C horizons) and where infiltration, evapotranspiration, and vertical and lateral flows occur; groundwater storage, to account for water flowing in the deep C horizon down to the bedrock or laterally within the deeper subsurface; and riparian "buffer zone" storage, to simulate the mixing of waters from the soil and the drift upon entering the stream. The buffer zone is meant to represent the "near-stream" Bh podzols that surround the stream network [see *Gillin et al.*, 2015], where a persistent water table exists [*Gannon et al.*, 2014].

A fundamental assumption of our modeling approach is that the average properties of each storage compartment in the model are perfectly reproduced by the corresponding outflows (e.g., the average deuterium content and age distributions of the soil storage are the same as the soil discharge). Such a configuration naturally emerges when mixing processes and macrodispersion prevail over advective transport [see *Benettin et al.*, 2013b]. The above assumption is commonly referred to as random sampling (RS) [*Benettin et al.*, 2013a; *Harman*, 2015], to stress that the outflows are considered representative samples of the corresponding storages. The RS assumption provides two major advantages: (i) the age distributions can be computed through simple analytic formulations [*Botter et al.*, 2010; *Botter*, 2012], which only involve knowledge of the relevant fluxes and storage (see formulas reported in the supporting information) and (ii) outflow concentrations are equal to the average storage concentration and can be easily computed by means of mass balances (supporting information), with great computational improvements that enable the calibration of model parameters through Monte Carlo techniques. While the schematization of a catchment as a single RS system is typically unsatisfactory, the partitioning of a catchment into two or three RS compartments (arranged in series or in parallel) has proved to be effective at capturing the main short-term and long-term water quality dynamics in many real-world settings [e.g., *Bertuzzo et al.*, 2013; *Hrachowitz et al.*, 2015].

In the soil and groundwater compartments, we model the storage $W(t)$ as the sum of a dynamic storage $S(t)$ and a residual storage W_0, which is assumed to be constant for simplicity. Such a separation is necessary in hydrochemical models because the dynamic storage involved in the hydrologic balance is just a fraction of the storage which is involved in solute mixing [*Kirchner*, 2009; *Birkel et al.*, 2011]. The dynamic storage is computed along with the hydrologic model, while the residual component is assessed through calibration against isotopic data (see section 3.2).

The model implementation is briefly illustrated below and a more thorough description of the model is provided in the supporting information. The soil compartment includes infiltration from precipitation and snowmelt, evapotranspiration, and lateral and vertical flow generation. A threshold T_{th} of daily-mean air

Table 1. Constant Parameters

Parameter	Symbol	Value
Soil porosity	n	0.35
Root-zone depth (mm)	Z_r	500
Buffer area fraction (%)	f_{buf}	5
Buffer storage (mm H_2O)	W_{buf}	100

temperature T_a was used to distinguish between snowfall and rainfall. $T_a \geq T_{th}$ resulted in water infiltration into the soil, while $T_a < T_{th}$ resulted in snow accumulation. Snowmelt infiltration was determined using a Degree-Day approach [see *Rango and Martinec*, 1995; *Tobin et al*., 2013], which proves adequate to compute snowmelt flux as the product of a Degree-Day factor D_f and the temperature difference $T_a - T_{th}$. The dynamic soil storage S_{sl} was normalized by the root-zone pore volume to provide a dimensionless measure of soil wetness $s_{sl}(t) = S_{sl}(t)/(nZ_r)$, n and Z_r being porosity and average root-zone depth. Potential evapotranspiration was computed as the product between a reference value ET_{ref} and a temperature-based term that could account for daily and seasonal evapotranspiration patterns. Actual evapotranspiration ET was then obtained by limiting potential evapotranspiration when $s_{sl} < 0.5$. Lateral and vertical flows were simulated with a nonlinear storage-discharge relationship $L = as_{sl}^b$, where $L(t)$ represents the total water flux leaking out of the soil. A fraction $\beta(t)$ of the leakage was used to compute the lateral flow (which discharges directly into the buffer zone as soil discharge Q_{sl}), while the remaining $(1 - \beta(t))$ fraction was assumed to recharge the deeper groundwater system. To allow a higher fraction of water to move laterally when the catchment is wet (as supported by field observations) [*Gannon et al*., 2014], the partitioning term was computed as the product between a constant parameter and the soil wetness: $\beta(t) = \beta_0 \cdot s_{sl}(t)$. The δD isotopic composition measured in precipitation and snowmelt was used to characterize infiltrating water. Fractionation was assumed to be negligible, so the deuterium content of the soil storage $\overline{\delta D}_{W_{sl}}$ was kept as conservative. Due to the RS assumption, evapotranspiration and lateral and vertical flows were assigned at any time the same composition as the soil water storage. The groundwater storage component of the model accounts for water flowing in the deeper glacial drift deposit. The input flux to the deep system is the vertical flow from the shallow storage, characterized by its modeled isotopic composition. The only output of the system is groundwater flow Q_{gw}, which was modeled through the linear relationship $Q_{gw} = cS_{gw}$, where S_{gw} represents the dynamic component of the storage. Evapotranspiration is ignored in the groundwater compartment because roots have limited access to this zone. The RS scheme for groundwater storage implies that the isotopic composition of deep discharge is the same as the average groundwater storage $\overline{\delta D}_{W_{gw}}(t)$.

The buffer zone is designed to represents the mixing volume within the riparian area of the catchment, where soil water and groundwater mix upon entering the stream. Such area was estimated to be about 10–20% of the total catchment area [*Gillin et al*., 2015] and is mostly composed of near-stream Bh podzols. The soil has been shown to have a persistent water table averaging about 30 cm above the C horizon, with little variation over time [*Gannon et al*., 2014]. Hence, for the sake of simplicity, the modeled buffer zone storage W_{buf} was kept constant, implying that water entering the riparian area from the soil and drift deposits is essentially equal to water displaced from the riparian area as total streamflow $Q(t)$ (plus the little fraction of evapotranspiration that pertains the buffer area). In order to describe the riparian mixing dynamics as a simple mixing process based on the random-sampling scheme, a smaller extent of the buffer area was used because the riparian area is a transition zone and cannot be assumed as completely mixed. The extent of the buffer region basically controls the higher-frequency fluctuations of the isotopic signal, leaving the main seasonal pattern almost unchanged. Preliminary model runs suggested a plausible range of values from 3% to 8%, which prevents the modeled deuterium signal from being too erratic or damped. Hence, we selected an effective, intermediate value of 5%. All discharge Q is composed of water from the buffer area and due to the RS assumption it is characterized by a deuterium content δD_Q, which is the same as the average buffering zone storage $\overline{\delta D}_{W_{buf}}(t)$.

3.2. Calibration

Some of the transport model parameters were set a priori based on previous work [e.g., *Bailey et al*., 2014] or field-based observations from the catchment. The buffer zone storage parameter W_{buf} was estimated from the average water table of 30 cm measured in the near-stream Bh podzol [*Gannon et al*., 2014], resulting in about 100 mm of water equivalent depth. This value was confirmed by preliminary calibration runs. All the constant model parameters are reported in Table 1.

The remaining parameters were estimated through a Markov Chain Monte Carlo (MCMC) calibration procedure using $DREAM_{ZS}$ [*Vrugt et al*., 2009; *ter Braak and Vrugt*, 2008]. These comprise seven hydrologic

Table 2. Calibration Parameters[a]

Parameter	Symbol	Low. Bound	Upp. Bound	Calibrated
DD threshold temp. (°C)	T_{th}	−3	1	−1
DD factor (mm/d °C)	D_f	0.5	5	2.2
Reference ET (mm/d)	ET_{ref}	0.5	3	2.2
Leakage partitioning	β_0	0.5	1.5	1.1
SD exponent sl	b	0	30	12.5
SD coeff. sl (mm/d)	a	10^0	10^5	$10^{2.05}$
SD coefficient gw	c	10^{-2}	10^2	$10^{-0.51}$
Resid. storage sl (mm H_2O)	W_{sl}	100	1000	250
Resid. storage gw (mm H_2O)	W_{gw}	100	5000	750

[a]SD = storage-discharge relationship, DD = Degree-Day, sl and gw refer to the soil layer and groundwater, respectively.

parameters (T_{th} and D_f for the Degree-Day model, the constants a, b, and c for the storage-discharge relationships, β_0 for the leakage partitioning, and ET_{ref} for evapotranspiration) and two transport parameters (the residual storages W_{sl} and W_{gw}), as summarized in Table 2. Following the procedure used in *Benettin et al*. [2015b], the hydrologic and transport parameters were calibrated separately. Hydrologic parameters were calibrated against daily log-discharge data over the 4 year period from November 2006 to October 2010. Log-discharge measurements were chosen for calibration to favor the reproduction of very low flows, which otherwise would be completely disregarded by the calibration as runoff varies up to 3 orders of magnitude. The model was run at hourly time steps and then aggregated to provide average daily values. Residual storage parameters were calibrated against weekly deuterium measurements available over the period November 2006 to May 2009. The weekly measurements may not capture all the high-frequency dynamics occurring during high flows. However, the samples were collected during very different hydrologic conditions and they did not show evidence of large fluctuations in stream deuterium content, suggesting that the buffering effect of the riparian zones may filter out most of the higher-frequency dynamics. The MCMC calibrations were performed using a standard log likelihood function with increased residuals standard deviations (that account for observed residuals correlation) [*Benettin et al*., 2015b].

3.3. Chemical Kinetics for Silicon and Sodium

The calibrated hydrochemical model provides fluxes and storages which are the basis for the computation of time-variant TTDs (supporting information). Hence, the travel time information resulting from the calibrated model can be used to implement first-order chemical kinetics, which are suitable for characterizing the stream concentration of solutes produced by mineral weathering [*Maher*, 2011].

Due to primary mineral weathering processes, the immobile water in contact with the soil matrix is enriched in mineral solutes. When a water parcel travels within subsurface environments and interacts with the minerals and/or immobile water (Figure 5), the underlying solute concentration gradients trigger mass transfer processes through which mineral weathering products are transferred to the water. The travel time T represents the time available for solute transfer and thus is assumed as the main driver of the process. It is assumed that the solution concentration c of the traveling parcels changes through time according to a first-order kinetics toward the immobile-phase equilibrium concentration C_{eq} [*Maher*, 2011]:

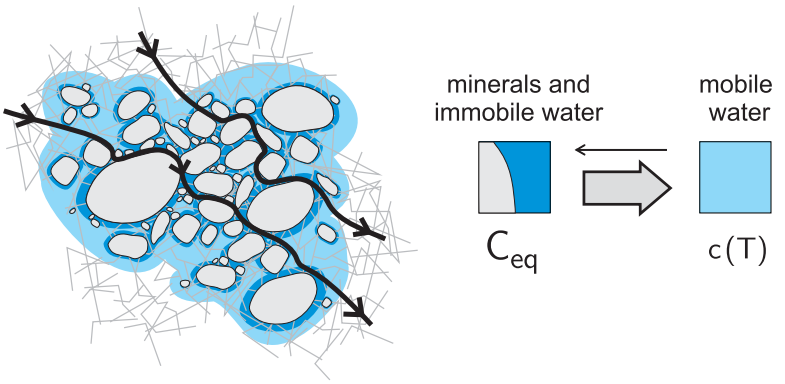

Figure 5. Graphical representation of the solute exchange between the mobile water and the minerals.

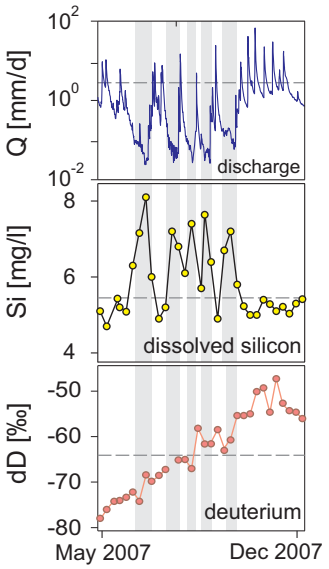

Figure 6. Example of dry summer period where the stream chemical composition is influenced by seeps. (middle) Silicon stream concentration increases during very low flows, while (bottom) deuterium content shows no correlation with discharge. The dashed lines indicate the long-term average value for each data set.

$$\frac{dc(T)}{dT} = k\,(c(T) - C_{eq})\,, \tag{1}$$

where k is an effective, catchment-scale kinetic constant [1/T]. Equation (1) is the analog of the Mass-Response Function (MRF) approach to basin-scale transport processes [*Rinaldo et al.*, 1989; *Botter et al.*, 2008, 2009]. When the initial concentration of the water parcel $c(0)$ is negligible (e.g., for purely geogenic solutes), the solution to equation (1) reads

$$c(T) = C_{eq}\,(1 - e^{-kT}). \tag{2}$$

Equation (2) implies that when the travel time T is short compared to $1/k$ (e.g., in the case of a short hydrologic flow path), the parcel concentration is much lower than C_{eq}. Conversely, for travel times that are significantly longer than $1/k$, the parcel concentration reaches the equilibrium value ($c \approx C_{eq}$). Note that the dissolution process is influenced by a number of relevant local factors, such as pH and temperature [see *Maher*, 2011], but, in large and complex domains like subsurface environments, flow path heterogeneity is speculated to reduce the effect of spatial gradients in local factors [*Botter et al.*, 2005]. Hence, when the catchment scale is larger than the correlation scale of heterogeneous attributes, the description of the emergent transport processes can be achieved through effective, spatially uniform parameters (k and C_{eq}). When considering the whole distribution of parcels that contribute to discharge at any time, the fraction that leaves the catchment with age T can be quantified through the (backward) travel time distribution $p_Q(T,t)$ [*Rinaldo et al.*, 2011; *Botter et al.*, 2011]. The resulting streamflow concentration is thus given by integration over all ages T:

$$C(t) = \int_0^\infty C_{eq}\,(1 - \exp^{-kT})\,p_Q(T,t)\,dT\,, \tag{3}$$

which can be directly used to compute silicon and sodium concentration at the catchment outlet.

An improved representation of the observed concentration signal can be achieved when the presence of the seeps is explicitly accounted for, as seeps are an expression of water discharged from unique flow paths. Seep flow at WS3 is persistently characterized by higher concentrations of solutes such as Na^+, Ca^{2+}, and H_2SiO_4, liberated during mineral weathering reactions [*Zimmer et al.*, 2013]. Some seeps are high in other metals of weathering origin such as Mn^{2+}. These patterns may reflect particular pathways that bring water in contact with fresh mineral surfaces characterized by a distinct mineral composition. Note that seep flow contribution to discharge is negligible most of the time, but it can dominate river hydrochemistry during extremely low flows (few weeks per year). Hence, seep flow is relatively unimportant in the yearly solute mass balance, although its presence is visible in the concentration time series during dry summer periods (Figure 6). Silicon stream concentration increases considerably when the hydrograph is controlled by the seeps, while isotope data are not correlated with discharge (Figure 6). Such a pattern suggests that seep flow water has not a different age, but it may intersect zones where the more weatherable minerals are still present, resulting in higher concentrations of silicon and sodium. This process can be simulated by assuming that a constant amount Q_{seep} of the calculated discharge originates in the seeps. The related seep concentration is computed through equation (3) using a different value for the equilibrium concentration (C_{seep}). Q_{seep} can be extracted by looking at typical values of discharge during the driest summer days, when seeps dominate the hydrograph (Figure 2a), and was set to 0.15 mm/d (or equal to total discharge when discharge is lower than 0.15 mm/d).

When the effect of the seeps is accounted for, streamflow concentration can be computed from equation (3) by replacing the constant term C_{eq} with the weighted average $[(Q(t) - Q_{seep}) \cdot C_{eq} + Q_{seep} \cdot C_{seep}]/Q(t)$. The chemograph is thus simulated using three parameters (C_{eq}, C_{seep}, and k). The kinetic constant k needs

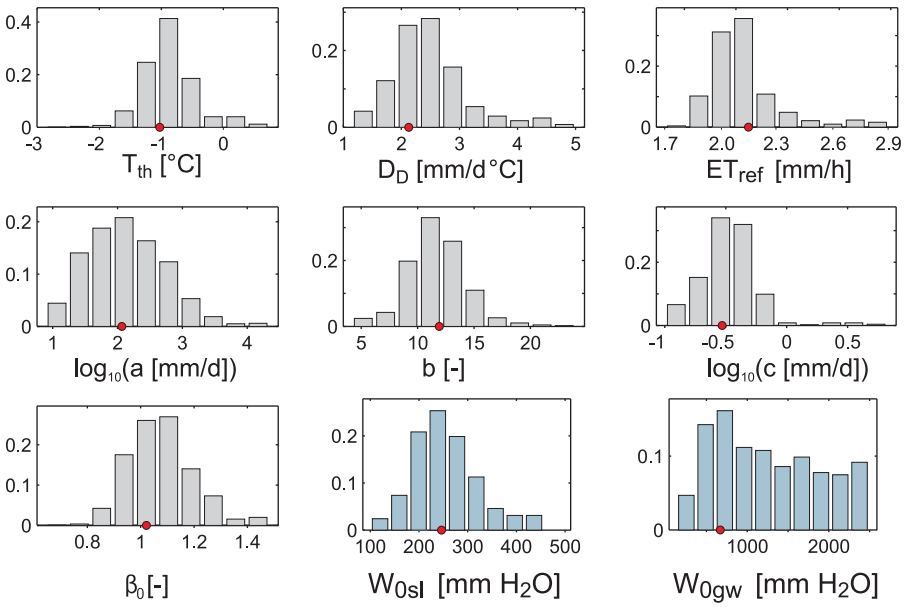

Figure 7. Posterior distributions of hydrologic (grey bars) and transport (blue bars) parameters, reported in Table 2. Red dots correspond with the calibrated values.

calibration, while C_{eq} and C_{seep} can be derived from available observations at seeps and at the catchment outlet during low flow conditions, when it can be reasonably assumed that solute concentration has reached equilibrium. However, all three model parameters were calibrated in the simulation to check whether optimal C_{eq} and C_{seep} values are consistent with those suggested by the measurements. Optimal parameter values were obtained through MCMC calibration during March 2008 to March 2010, using $DREAM_{ZS}$ [*ter Braak and Vrugt*, 2008; *Vrugt et al*., 2009]. The remaining 12 years of measurements were used for the validation of the model.

4. Results

The calibration procedure of the transport model resulted in relatively narrow posterior distributions of the parameter values (Figure 7), except for the groundwater residual storage W_{0gw}, which shows no clear upper bound. Such uncertainty, however, has almost no impact on the model results, as explained below and in section 5. Modeled discharge is reported in Figures 8a and 8b, where 95% confidence intervals are plotted against measurements. A simple sensitivity analysis showed that the hydrologic model is most sensitive to the snow model parameters. This finding is not surprising as occasionally discharge peaks are missed because the precipitation event was interpreted by the snow module as snowfall accumulation. In any case, these events are quite rare and overall the model is able to reproduce the observed discharge signal quite well. The calibrated model has Nash-Sutcliffe efficiency NS = 0.78 for log-discharge and NS = 0.75 for discharge. Validation during January 2000 to May 2006 resulted in NS = 0.78 for log-discharge and NS = 0.73 for discharge, indicating a certain robustness of the calibrated values. The partitioning of streamflow into soil and groundwater sources (not shown) reveals that, annually, only 25% of the discharge originates from deep groundwater, but it accounts for more than 95% of the flow during dry summer periods. Modeled snowfall accumulation is compared to measurements in Figure 8c and indicates that the model captures the timing pattern of snow accumulation and melt.

The calibrated deuterium signal is compared to measurements in Figure 8d. Both weekly and biweekly measurements are reported in the plot to provide an idea of measurement variability. As biweekly data are available over a longer period, they can serve for validating the model during May 2009 to October 2010. The simulated signal features both the seasonal and higher-frequency observed fluctuations. The model predicts higher deuterium contents during March–April 2009, probably related to the overestimation of snow accumulation during the previous winter and to the uncertainty in the related snowmelt isotopic composition. Nevertheless, the model prediction during the subsequent snowmelt season (validation

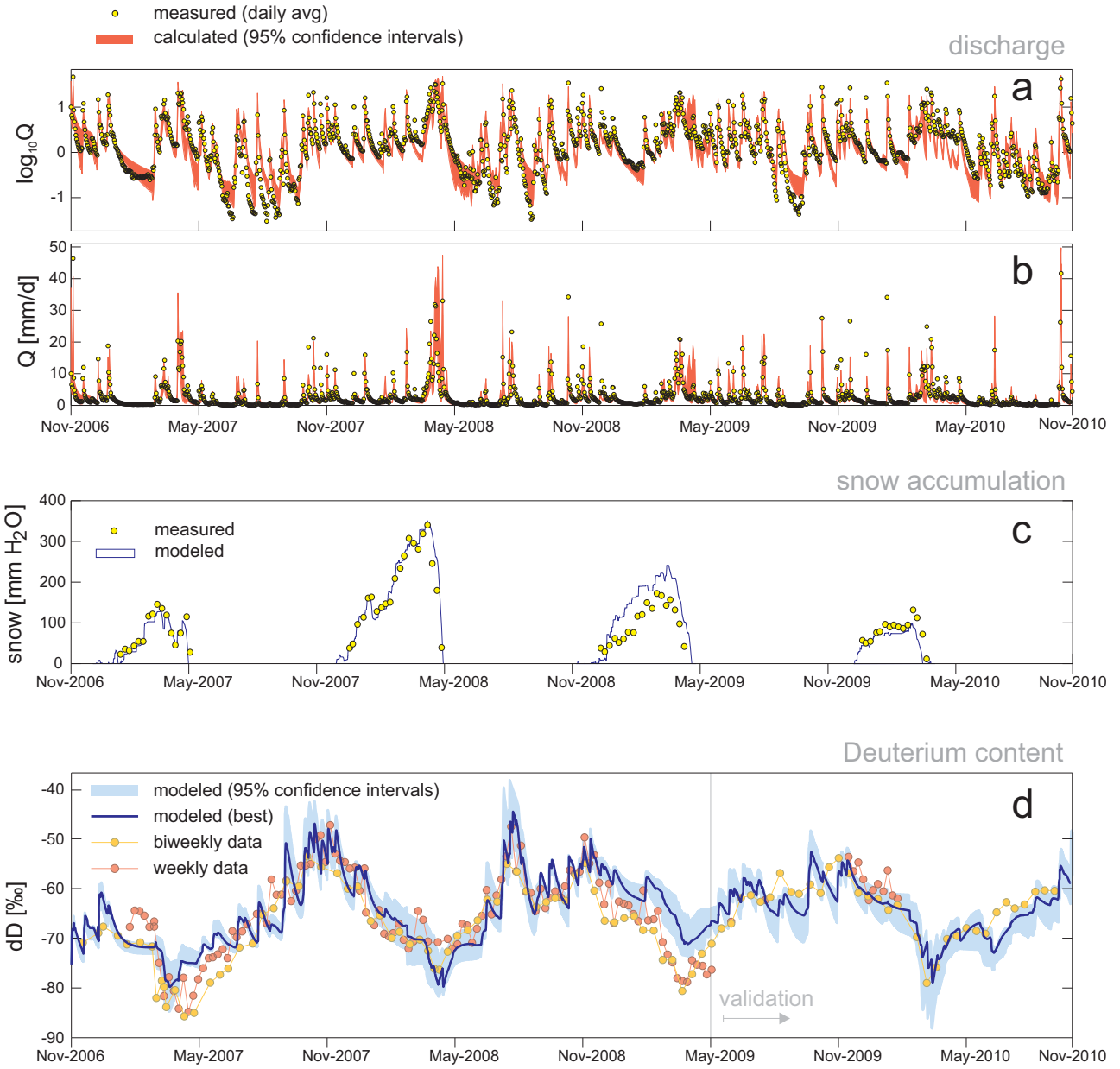

Figure 8. Model performance for (a) log-discharge, (b) discharge, (c) snow accumulation, and (d) streamflow isotopic composition.

period, spring 2010) is deemed quite accurate. Overall, the NS efficiencies of the 95% confidence interval simulations are in the range 0.44–0.62. Given the simple tools used to model rather complex processes like snowmelt and forest transpiration, the model results are considered satisfactory.

The travel time distributions that underly the model results were computed by aggregating fluxes to daily averages and using the analytical solutions for the random-sampling age-selection scheme [e.g., *Benettin et al.*, 2013a, Appendix A]. The procedure is detailed in the supporting information. The uncertainty in the groundwater residual storage size (Figure 7) induces some uncertainty in the longer travel times, with strong impact on the mean of the distributions. The use of percentiles like the median travel time (i.e., the age that is not exceeded by 50% of the discharge) is then more suitable to characterize water age because it does not need knowledge of the older (and more uncertain) components of the distributions. This also makes the age estimate consistent with the possible presence of very old water particles which may be revealed by other tracers [see *Stewart et al.*, 2012]. According to the model, median travel time changes

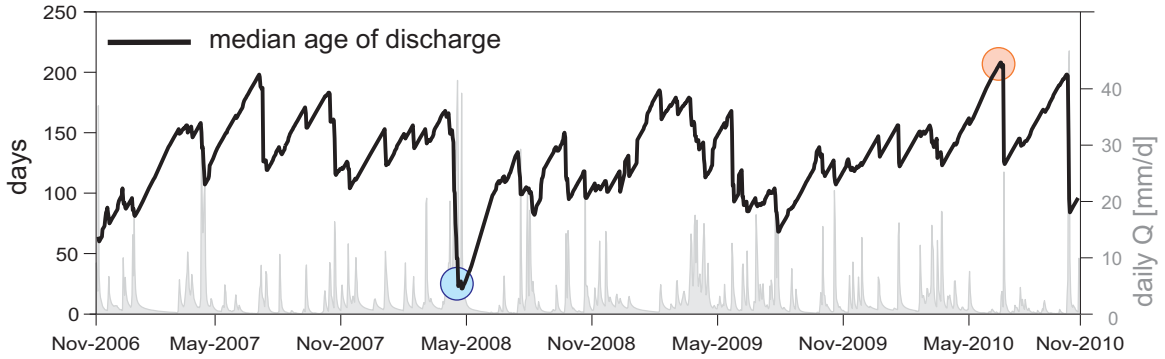

Figure 9. Evolution of the simulated median age of discharge during a 4 year period. The red and blue circles denote the dry and wet periods explored in Figure 10.

during the year (Figure 9), ranging from 40–60 days during wet periods (e.g., after intense storms, or during spring snowmelt) to 180–200 days during dry summers and winter snow accumulation periods. Figure 9 also shows the essence of nonstationarity, i.e., that storm events cause a drop in the median travel time because they typically mobilize younger water particles. The different features displayed by the TTDs during different periods are shown in Figure 10, where selected distributions are reported. The selected TTDs are probability density functions (pdf) and cumulative distribution functions (CDF) computed for each day during a 2 week wet and a 2 week dry period. The wet period corresponds to an intense storm event during snowmelt in April 2008. The corresponding modeled TTDs are largely composed of younger waters, although half of the released particles are nonevent water that proves older than 20 days. The dry period corresponds to the end of a long recession in June 2009 and its dynamics are similar to those of all prolonged recessions. Young water is almost entirely absent due to the dry antecedent weeks, and the most significant contribution of relatively younger water comes from storm events recorded 60–80 days prior to that period. The age estimates may be affected by the relatively coarse sampling frequency of the deuterium data set, so the degree of time-variance may be even greater, while the ordinary age dynamics, which are responsible of the clear sinusoidal pattern in the stream deuterium content, are expected to remain unchanged.

The calibrated values of the kinetic parameters (Table 3) were used to calculate variations in Si and Na concentration over the 14 year period 1998–2012 (Figure 11). The simulated time series is generally able to reproduce well the main features of the measured signal, including—remarkably—the dilution during stormflow, the increase in concentration during recession, and the positive peaks during the periods dominated by the seep flow. NS efficiency over the 14 year period is 0.63 for both solutes, with NS on individual years ranging from 0.21 to 0.81. The solute modeled concentration can be directly used to compute solute export from the catchment. A simple estimate of mass fluxes (reported in the supporting information,

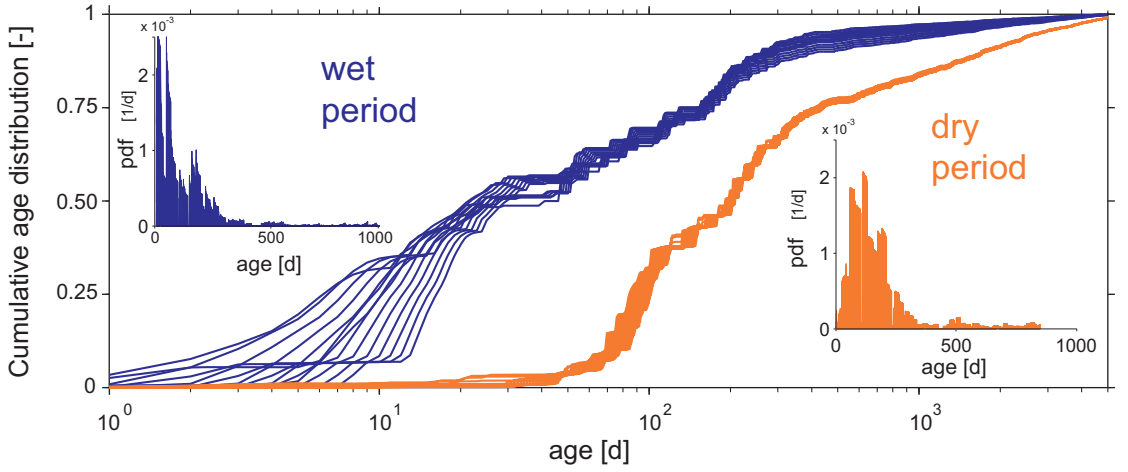

Figure 10. Cumulative TTDs of discharge, during the 2 weeks wet and 2 weeks dry periods indicated in Figure 9. The insets also report the corresponding pdfs.

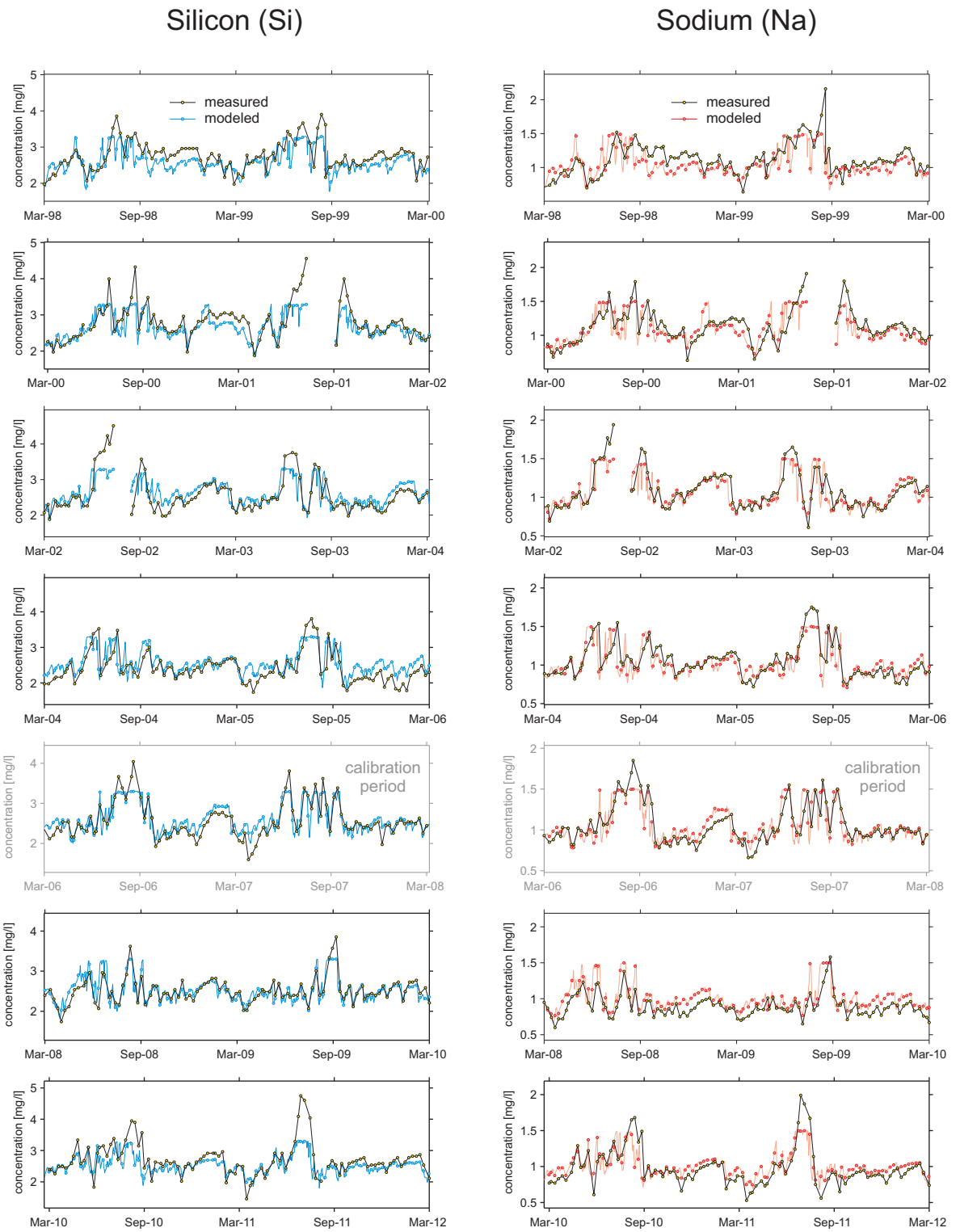

Figure 11. Fourteen year simulation of silicon and sodium concentration using the TTD-based approach.

Section S1) confirms that the periods with highest Si and Na concentration have a negligible impact on the solute mass balance, because they occur during extremely low flows. Calibrated equilibrium and seep concentrations for both solutes are consistent with the value of measured concentration during late recessions, suggesting that calibration may not be needed for those parameters.

Table 3. Kinetic Parameters

Parameter	Symbol	Value (Si)	Value (Na)
Kinetic. const. (d)	$1/k$	13	10
Equil. conc. (mg/L)	C_{eq}	2.4	0.95
Seep conc. (mg/L)	C_{seep}	3.4	1.5

5. Discussion

The fast hydrologic response simulated by the model relies on a storage-discharge relation within the soil compartment. The nonlinearity of such a relation at HBEF can be attributed to the spatial patterns of streamflow generation, where different soil units are activated at different storage thresholds [*Detty and McGuire*, 2010a, 2010b; *Gannon et al*., 2014]. Even though the catchment is characterized by heterogeneity in the soil distribution [*Gillin et al*., 2015] and complex spatial patterns in the stream solute concentration [*Zimmer et al*., 2013; *McGuire et al*., 2014], the integrated hydrochemical response of the watershed can be addressed using a lumped parameter approach at the catchment scale. Use of this approach is possible because of the integration power of the riparian areas and the stream network [*Rinaldo and Rodriguez-Iturbe*, 1996], which efficiently mix waters originating from spatially distinct sources within the catchment [*Bormann and Likens*, 1967; *Likens*, 2013]. The same approach, however, may not hold in settings where heterogeneity in the solute source or biogeochemical properties has a characteristic scale comparable to the catchment size.

The model allows for the estimate of the catchment storage involved in solute mixing within each compartment (soil, groundwater, and buffer region). Estimated soil storage is, on average, 380 mm water equivalent depth. Depending on the value of the porosity n, the storage estimated by the model would require a soil depth of about 120–140 cm (with $n \in [0.3, 0.4]$), which corresponds to the entire O-B horizons plus an additional 50–70 cm within the upper portion of the C horizon. This result implies that the lateral flows estimated by the transport model originate within the upper 150 cm of the soil and the glacial materials, indicating some active involvement of the upper C horizon in the short-term solute circulation. In addition to soil storage, there is substantial storage within glacial materials which provides a small contribution to streamflow, yet has important implications for catchment biogeochemistry. Deep groundwater storage estimates indicate a storage size of about 760 mm water equivalent, which suggests the presence of contributing water in the glacial material down to at least 3 m depth. These results are corroborated by recent ground-penetrating radar surveys and boreholes that suggest glacial deposits may be up to 5–8 m thick in places within the catchment. However, the depth is less constrained in the model because higher values for groundwater storage would provide similar deuterium, silicon, and sodium dynamics in the groundwater flow. The difficulty in constraining the deep catchment storage is a typical problem in this type of study [see *Stewart et al*., 2012; *Benettin et al*., 2015b], that deals with the very long transport time scales of groundwater compared to the short-term input variability and reaction kinetics. The uncertainty in determining the deep water storage size induces some degree of uncertainty in the longer travel times but leaves the estimate of younger water, which is responsible for most of the observed dynamics in water quality, almost unchanged.

The kinetic constant k allows a rough estimate of mass transfer time scales for weathering processes. For both silicon and sodium, the time scale (quantified by $1/k$) is about 10 days, which suggests that the driver of the streamflow concentration dynamics is the relative abundance of water younger than about 30 days. When a notable fraction of water characterized by short contact times with the immobile phase reaches the stream (e.g., right after a storm), the overall streamflow concentration decreases. The opposite holds during dry periods, when most of the water traveled much longer than 30 days and exits the catchment at the equilibrium concentration. When flows are extremely low, the influence of the seeps further increases the streamflow concentration, as suggested by *Zimmer et al*. [2013].

The estimate of streamflow age and transport time scales, although based on accurate model results on both flow and transport, should be taken with some caution. It was beyond the scope of this study comparing streamflow age estimates from different models and tracers, and it cannot be excluded that different model structures (e.g., with a different conceptualization of the riparian areas) could lead to different values of the median travel time. However, the results of silicon and sodium simulations show that the relative variations in streamflow age, related to variations in the hydrologic drivers, prove reliable. Hence, estimates of absolute age may be somewhat different when using different models or tracers, but relative temporal variations are expected to be as pronounced as shown in this study.

The early work by *Johnson et al*. [1981] presented a simple model to explain longitudinal patterns in stream solute composition that stated that mineral weathering contributions increased with lengthening water age

or flow path length in the system. While *Johnson et al*. [1981] did not attempt to differentiate or quantify water age or flow path length, our results are consistent with this classic interpretation and yield a much more detailed picture of how age and subsurface structure and flow paths may result in temporal patterns in weathering-derived solutes. Sodium and silicon are relatively unaffected by processes other than weathering. Na is little taken up by plants and is not much stored in the soil on the cation-exchange complex. Si is taken up by plants, to a limited degree, and is stored in secondary materials—phytoliths and maybe neoclay minerals. But these dynamics may be relatively small compared to the dissolution dynamics. The fact that the model works suggests this is true. The main advantage of the method relies on its ability to incorporate the hydrologic variations of the system, as implied by the use of time-variable TTDs that explicitly take into account the variability of hydrologic drivers like precipitation, storage, and discharge. Overall, our results suggest that silicon and sodium stream concentrations at HBEF can be significantly impacted and properly predicted by catchment-scale hydrologic controls.

The use of spatially integrated chemical kinetics was here tested at HBEF WS3, but due to the simple and general character of the involved equations, it could be applied to any setting where the effect of spatial heterogeneity can be integrated out (hence allowing the use of catchment-scale TTDs and effective geochemical parameters). The application can also be extended to other solutes from geogenic and atmospheric sources, like, e.g., calcium and magnesium. However, these are required nutrients that are actively taken up by plants and have significant (and perhaps temporally dynamic) pools on the soil cation-exchange complex. In such cases, the outlined method may be still used as a test to screen the relative importance of hydrologic controls on solute export.

6. Conclusions

Despite the challenge represented by modeling the hydrochemistry of a small catchment with intense evapotranspiration and snowmelt, the coherent framework to model flow and transport developed in this paper was able to reproduce a number of catchment dynamics including runoff, snow accumulation, streamflow isotopic content, and silicon and sodium concentrations. The results, used as a tool to screen assumptions about the leading processes, suggest a significant presence of water in the drift deposit, which is actively involved in solute circulation and allowed the estimate of solute transport temporal scales.

The accuracy in reproducing the observed streamflow concentrations is a prerequisite to estimate catchment TTDs. Our results indicate that median travel times can range from 50 to 200 days depending on catchment wetness conditions. Even though longer travel times are typically difficult to constrain, shorter travel times are more identifiable because they are responsible for the observed dynamics in stream hydrochemistry of this catchment.

The estimated travel times proved crucial for describing the variation of geogenic solutes in surface waters, like those derived by weathering processes. The agreement between modeled and observed silicon and sodium concentrations in stream water during a 14 year period, in fact, suggests that the dynamic nature of streamflow generation processes (and of the embedded TTDs) is one of the main drivers of water quality dynamics at HBEF. Overall, our results support the coupled use of long-term solute measurements and transport models to quantify catchment-scale solute mixing and allow a rigorous assessment of hydrologic and biogeochemical processes in complex environments like catchments.

Appendix A: Isotope Sampling Procedure and Analyses

Bulk precipitation was sampled in a clearing within the boundary of WS3. The precipitation collector was mounted on a post 1.5 m above the ground surface and consisted of a 15 cm-diameter polyvinyl chloride (PVC) tube lined with a polyethylene bag. When precipitation fell mostly as rain, a small amount ($\sim$10 mL) of mineral oil was added to the bag to prevent evaporation during the 2 week sampling interval. The precipitation sample was collected by cutting a hole in the bottom of the bag and letting the accumulated water drain into a sample vial, while being careful to exclude the thin layer of mineral oil on the surface. When precipitation fell mostly as snow, no mineral oil was added to the bags, and the samples were melted at room temperature before decanting. Snowmelt from the bottom of the snowpack was collected with three 1.1 m^2 lysimeters located in the forest adjacent to the clearing where precipitation was collected. The

snowmelt lysimeters were constructed of 6 mm-thick PVC trays placed on the surface of the forest floor [see *Campbell et al*., 2007]. Snowmelt water drained by gravity through a PVC pipe into a sample collection bottle housed in a storage container that was buried in the ground. The storage container was insulated to prevent the sample from freezing and could be accessed by digging through the overlying snowpack. The biweekly snowmelt sample consisted of a composite sample from the three lysimeters. Stream water samples were collected at the WS3 outlet several meters upstream from the ponding basin for the weir. All water isotope samples were stored in 20 mL glass vials with conical caps to eliminate headspace. Shortly after collection, the vials were dipped in paraffin wax to seal them until analysis. Samples from November 2006 to November 2008 were analyzed for hydrogen isotopes at the University of New Hampshire using the zinc reduction method (precision of 0.4‰) following *Coleman et al*. [1982]. After that, samples were analyzed at Plymouth State University with cavity ring-down spectroscopy (precision of 0.8%) following *Lis et al*. [2008]. A subset of samples using both methods indicated that the median difference in deuterium was 3%.

Acknowledgments

Data to support this study are provided by the Hubbard Brook Ecosystem Study and can be obtained through the website www.hubbardbrook.org or upon request. The authors thank Don Ross and J.P. Gannon for an early review of the manuscript, and Christian Birkel and two anonymous reviewers for the useful comments provided. K.M. and S.B. thank support from NSF EAR 1014507. A.R. thanks support from SNF-FNS Projects 200021-124930/1 and 200021-135241. Funding to G.L. for the long-term precipitation and stream water chemistry was provided by the NSF, including the LTER and LTREB programs, and The A.W. Mellon Foundation. Hubbard Brook Experimental Forest is operated and managed by the U.S. Forest Service, Northern Research Station, Newton Square, PA.

References

Asano, Y., T. Uchida, and N. Ohte (2003), Hydrologic and geochemical influences on the dissolved silica concentration in natural water in a steep headwater catchment, *Geochim. Cosmochim. Acta*, *67*(11), 1973–1989, doi:10.1016/S0016-7037(02)01342-X.

Aubert, A., et al. (2013), Solute transport dynamics in small, shallow groundwater-dominated agricultural catchments: Insights from a high-frequency, multisolute 10 yr-long monitoring study, *Hydrol. Earth Syst.*, *17*(4), 1379–1391, doi:10.5194/hess-17-1379-2013.

Bailey, A. S., J. W. Hornbeck, J. L. Campbell, and C. Eager (2003), Hydrometeorological database for Hubbard Brook Experimental Forest: 1955–2000, Tech. Rep. NE-305, U.S. Dept. of Agric., For. Serv., Northeast. Res. Stn., Newtown Square, Pa.

Bailey, S., D. Buso, and G. Likens (2003), Implications of sodium mass balance for interpreting the calcium cycle of a forested ecosystem, *Ecology*, *84*(2), 471–484, doi:10.1890/0012-9658(2003)084[0471:IOSMBF]2.0.CO;2.

Bailey, S., P. Brousseau, K. McGuire, and D. Ross (2014), Influence of landscape position and transient water table on soil development and carbon distribution in a steep, headwater catchment, *Geoderma*, *227*, 279–289, doi:10.1016/j.geoderma.2014.02.017.

Benettin, P., Y. van der Velde, S. E. A. T. M. van der Zee, A. Rinaldo, and G. Botter (2013a), Chloride circulation in a lowland catchment and the formulation of transport by travel time distributions, *Water Resour. Res.*, *49*, 4619–4632, doi:10.1002/wrcr.20309.

Benettin, P., A. Rinaldo, and G. Botter (2013b), Kinematics of age mixing in advection-dispersion models, *Water Resour. Res.*, *49*, 8539–8551, doi:10.1002/2013WR014708.

Benettin, P., A. Rinaldo, and G. Botter (2015a), Tracking residence times in hydrological systems: Forward and backward formulations, *Hydrol. Processes*, doi:10.1002/hyp.15034, in press.

Benettin, P., J. W. Kirchner, A. Rinaldo, and G. Botter (2015b), Modeling chloride transport using travel time distributions at Plynlimon, Wales, *Water Resour. Res.*, *51*, 3259–3276, doi:10.1002/2014WR016600.

Bertuzzo, E., M. Thomet, G. Botter, and A. Rinaldo (2013), Catchment-scale herbicides transport: Theory and application, *Adv. Water Resour.*, *52*(0), 232–242, doi:10.1016/j.advwatres.2012.11.007.

Birkel, C., C. Soulsby, and D. Tetzlaff (2011), Modelling catchment-scale water storage dynamics: Reconciling dynamic storage with tracer-inferred passive storage, *Hydrol. Processes*, *25*(25), 3924–3936, doi:10.1002/hyp.8201.

Birkel, C., C. Soulsby, D. Tetzlaff, S. Dunn, and L. Spezia (2012), High-frequency storm event isotope sampling reveals time-variant transit time distributions and influence of diurnal cycles, *Hydrol. Processes*, *26*(2), 308–316, doi:10.1002/hyp.8210.

Birkel, C., C. Soulsby, and D. Tetzlaff (2015), Conceptual modelling to assess how the interplay of hydrological connectivity, catchment storage and tracer dynamics controls nonstationary water age estimates, *Hydrol. Processes*, *29*(13), 2956–2969, doi:10.1002/hyp.10414.

Bormann, F. H., and G. E. Likens (1967), Nutrient cycling, *Science*, *155*(3761), 424–429, doi:10.1126/science.155.3761.424.

Botter, G. (2012), Catchment mixing processes and travel time distributions, *Water Resour. Res.*, *48*, W05545, doi:10.1029/2011WR011160.

Botter, G., E. Bertuzzo, A. Bellin, and A. Rinaldo (2005), On the Lagrangian formulations of reactive solute transport in the hydrologic response, *Water Resour. Res.*, *41*, W04008, doi:10.1029/2004WR003544.

Botter, G., F. Peratoner, M. Putti, A. Zuliani, R. Zonta, A. Rinaldo, and M. Marani (2008), Observation and modeling of catchment-scale solute transport in the hydrologic response: A tracer study, *Water Resour. Res.*, *44*, W05409, doi:10.1029/2007WR006611.

Botter, G., E. Milan, E. Bertuzzo, S. Zanardo, M. Marani, and A. Rinaldo (2009), Inferences from catchment-scale tracer circulation experiments, *J. Hydrol.*, *369*(34), 368–380, doi:10.1016/j.jhydrol.2009.02.012.

Botter, G., E. Bertuzzo, and A. Rinaldo (2010), Transport in the hydrologic response: Travel time distributions, soil moisture dynamics, and the old water paradox, *Water Resour. Res.*, *46*, W03514, doi:10.1029/2009WR008371.

Botter, G., E. Bertuzzo, and A. Rinaldo (2011), Catchment residence and travel time distributions: The master equation, *Geophys. Res. Lett.*, *38*, L11403, doi:10.1029/2011GL047666.

Burt, T. (1994), Long-term study of the natural environment —Perceptive science or mindless monitoring?, *Prog. Phys. Geogr.*, *18*(4), 475–496, doi:10.1177/030913339401800401.

Campbell, J. L., M. J. Mitchell, B. Mayer, P. M. Groffman, and L. M. Christenson (2007), Mobility of nitrogen-15-labeled nitrate and sulfur-34-labeled sulfate during snowmelt, *Soil Sci. Soc. Am. J.*, *71*, 1934–1944, doi:10.2136/sssaj2006.0283.

Cedarholm, D. (1994), Dominant soil water pathways on a northern New England forested hillslope, MS thesis, Univ. of N. H., Durham.

Clymans, W., G. Govers, E. Frot, B. Ronchi, B. Van Wesemael, and E. Struyf (2013), Temporal dynamics of bio-available Si fluxes in a temperate forested catchment (Meerdaal forest, Belgium), *Biogeochemistry*, *116*(1–3), 275–291, doi:10.1007/s10533-013-9858-9.

Coleman, M. L., T. J. Shepherd, J. J. Durham, J. E. Rouse, and G. R. Moore (1982), Reduction of water with zinc for hydrogen isotope analysis, *Anal. Chem.*, *54*(6), 993–995, doi:10.1021/ac00243a035.

Conley, D. J., G. E. Likens, D. C. Buso, L. Saccone, S. W. Bailey, and C. E. Johnson (2008), Deforestation causes increased dissolved silicate losses in the Hubbard Brook Experimental Forest, *Global Change Biol.*, *14*(11), 2548–2554, doi:10.1111/j.1365-2486.2008.01667.x.

Dansgaard, W. (1964), Stable isotopes in precipitation, *Tellus*, *16*(4), 436–468, doi:10.1111/j. 2153-3490.1964.tb00181.x.

Davies, J., K. Beven, A. Rodhe, L. Nyberg, and K. Bishop (2013), Integrated modeling of flow and residence times at the catchment scale with multiple interacting pathways, *Water Resour. Res.*, *49*, 4738–4750, doi:10.1002/wrcr.20377.

Detty, J. M., and K. J. McGuire (2010a), Threshold changes in storm runoff generation at a till-mantled headwater catchment, *Water Resour. Res.*, *46*, W07525, doi:10.1029/2009WR008102.
Detty, J. M., and K. J. McGuire (2010b), Topographic controls on shallow groundwater dynamics: Implications of hydrologic connectivity between hillslopes and riparian zones in a till mantled catchment, *Hydrol. Processes*, *24*(16), 2222–2236, doi:10.1002/hyp.7656.
Gannon, J. P., S. W. Bailey, and K. J. McGuire (2014), Organizing groundwater regimes and response thresholds by soils: A framework for understanding runoff generation in a headwater catchment, *Water Resour. Res.*, *50*, 8403–8419, doi:10.1002/2014WR015498.
Gat, J. R. (1996), Oxygen and hydrogen isotopes in the hydrologic cycle, *Annu. Rev. Earth Planet. Sci.*, *24*(1), 225–262, doi:10.1146/annurev.earth.24.1.225.
Gillin, C. P., S. W. Bailey, K. J. McGuire, and J. P. Gannon (2015), Mapping of hydropedologic spatial patterns in a steep headwater catchment, *Soil Sci. Soc. Am. J.*, *79*(2), 440–453, doi:10.2136/sssaj2014.05.0189.
Godsey, S. E., J. W. Kirchner, and D. W. Clow (2009), Concentration–discharge relationships reflect chemostatic characteristics of us catchments, *Hydrol. Processes*, *23*(13), 1844–1864, doi:10.1002/hyp.7315.
Harman, C., and M. Kim (2014), An efficient tracer test for time-variable transit time distributions in periodic hydrodynamic systems, *Geophys. Res. Lett.*, *41*, 1567–1575, doi:10.1002/2013GL058980.
Harman, C. J. (2015), Time-variable transit time distributions and transport: Theory and application to storage-dependent transport of chloride in a watershed, *Water Resour. Res.*, *51*, 1–30, doi:10.1002/2014WR015707.
Heidbuechel, I., P. A. Troch, S. W. Lyon, and M. Weiler (2012), The master transit time distribution of variable flow systems, *Water Resour. Res.*, *48*, W06520, doi:10.1029/2011WR011293.
Hooper, R. P., and C. A. Shoemaker (1986), A comparison of chemical and isotopic hydrograph separation, *Water Resour. Res.*, *22*(10), 1444–1454, doi:10.1029/WR022i010p01444.
Hornberger, G., T. Scanlon, and J. Raffensperger (2001), Modelling transport of dissolved silica in a forested headwater catchment: The effect of hydrological and chemical time scales on hysteresis in the concentration-discharge relationship, *Hydrol. Processes*, *15*(10), 2029–2038, doi:10.1002/hyp.254.
Hrachowitz, M., H. Savenije, T. A. Bogaard, D. Tetzlaff, and C. Soulsby (2013), What can flux tracking teach us about water age distribution patterns and their temporal dynamics?, *Hydrol. Earth Syst. Sci.*, *17*(2), 533–564, doi:10.5194/hess-17-533-2013.
Hrachowitz, M., O. Fovet, L. Ruiz, and H. H. G. Savenije (2015), Transit time distributions, legacy contamination and variability in biogeochemical 1/*f* scaling: How are hydrological response dynamics linked to water quality at the catchment scale?, *Hydrol. Processes*, doi:10.1002/hyp.10546, in press.
Ingraham, N. L. (1998), Isotopic variations in precipitation, in *Isotope Tracers in Catchment Hydrology*, edited by J. J. McDonnell and C. Kendall, chap. 3, pp. 87–118, Elsevier, Amsterdam, doi:10.1016/B978-0-444-81546-0.50010-0.
Johnson, C. E., A. H. Johnson, and T. G. Siccama (1991), Whole-tree clear-cutting effects on exchangeable cations and soil acidity, *Soil Sci. Soc. Am. J.*, *55*(2), 502–508, doi:10.2136/sssaj1991.03615995005500020035x.
Johnson, N. M., G. E. Likens, F. Bormann, and R. S. Pierce (1968), Rate of chemical weathering of silicate minerals in New Hampshire, *Geochim. Cosmochim. Acta*, *32*(5), 531–545, doi:10.1016/0016-7037(68)90044-6.
Johnson, N. M., G. E. Likens, F. Bormann, D. Fisher, and R. Pierce (1969), A working model for variation in stream water chemistry at Hubbard Brook Experimental Forest, New-Hampshire, *Water Resour. Res.*, *5*(6), 1353–1363, doi:10.1029/WR005i006p01353.
Johnson, N. M., C. T. Driscoll, J. S. Eaton, G. E. Likens, and W. H. McDowell (1981), Acid rain, dissolved aluminum and chemical weathering at the Hubbard Brook Experimental Forest, New Hampshire, *Geochim. Cosmochim. Acta*, *45*(9), 1421–1437, doi:10.1016/0016-7037(81)90276-3.
Kirchner, J., X. Feng, and C. Neal (2000), Fractal stream chemistry and its implications for contaminant transport in catchments, *Nature*, *403*(6769), 524–527, doi:10.1038/35000537.
Kirchner, J. W. (2009), Catchments as simple dynamical systems: Catchment characterization, rainfall-runoff modeling, and doing hydrology backward, *Water Resour. Res.*, *45*, W02429, doi:10.1029/2008WR006912.
Lawrence, G., and C. Driscoll (1990), Longitudinal patterns of concentration-discharge relationships in stream water draining the Hubbard Brook Experimental Forest, New-Hampshire, *J. Hydrol.*, *116*(1–4), 147–165, doi:10.1016/0022-1694(90)90120-M.
Likens, G. (2013), *Biogeochemistry of a Forested Ecosystem*, 3rd ed., Springer, N. Y.
Likens, G. E., and M. B. Davis (1975), Post-glacial history of Mirror Lake and its watershed in New Hampshire, USA: an initial report, *Verh. Internat. Verein. Limnol.*, *19*(2), 982–993.
Lindenmayer, D. B., et al. (2012), Value of long-term ecological studies, *Austral Ecol.*, *37*(7), 745–757, doi:10.1111/j.1442-9993.2011.02351.x.
Lis, G., L. I. Wassenaar, and M. J. Hendry (2008), High-precision laser spectroscopy D/H and $^{18}O/^{16}O$ measurements of microliter natural water samples, *Anal. Chem.*, *80*(1), 287–293, doi:10.1021/ac701716q.
Maher, K. (2010), The dependence of chemical weathering rates on fluid residence time, *Earth Planet. Sci. Lett.*, *294*(12), 101–110, doi:10.1016/j.epsl.2010.03.010.
Maher, K. (2011), The role of fluid residence time and topographic scales in determining chemical fluxes from landscapes, *Earth Planet. Sci. Lett.*, *312*, 48–58, doi:10.1016/j.epsl.2011.09.040.
McDonnell, J. J., and K. J. Beven (2014), Debates on water resources: The future of hydrological sciences: A (common) path forward? A call to action aimed at understanding velocities, celerities and residence time distributions of the headwater hydrograph, *Water Resour. Res.*, *50*, 5342–5350, doi:10.1002/2013WR015141.
McGuire, K., M. Weiler, and J. McDonnell (2007), Integrating tracer experiments with modeling to assess runoff processes and water transit times, *Adv. Water Resour.*, *30*(4), 824–837, doi:10.1016/j.advwatres.2006.07.004.
McGuire, K. J., and G. E. Likens (2011), *Historical Roots of Forest Hydrology and Biogeochemistry*, vol. 216, chap. 1, pp. 3–26, Springer, Heidelberg, Germany.
McGuire, K. J., and J. J. McDonnell (2006), A review and evaluation of catchment transit time modeling, *J. Hydrol.*, *330*(3–4), 543–563, doi:10.1016/j.jhydrol.2006.04.020.
McGuire, K. J., C. E. Torgersen, G. E. Likens, D. C. Buso, W. H. Lowe, and S. W. Bailey (2014), Network analysis reveals multiscale controls on streamwater chemistry, *Proc. Natl. Acad. Sci. U. S. A.*, *111*(19), 7030–7035, doi:10.1073/pnas.1404820111.
McMillan, H., D. Tetzlaff, M. Clark, and C. Soulsby (2012), Do time-variable tracers aid the evaluation of hydrological model structure? A multimodel approach, *Water Resour. Res.*, *48*, W05501, doi:10.1029/2011WR011688.
Neal, C., et al. (2012), High-frequency water quality time series in precipitation and streamflow: From fragmentary signals to scientific challenge, *Sci. Total Environ.*, *434*(SI), 3–12, doi:10.1016/j.scitotenv.2011.10.072.
Peters, N. E., D. A. Burns, and B. T. Aulenbach (2014), Evaluation of high-frequency mean streamwater transit-time estimates using groundwater age and dissolved silica concentrations in a small forested watershed, *Aquat. Geochem.*, *20*(2–3), 183–202, doi:10.1007/s10498-013-9207-6.

Queloz, P., L. Carraro, P. Benettin, G. Botter, A. Rinaldo, and E. Bertuzzo (2015), Transport of fluorobenzoate tracers in a vegetated hydrologic control volume: 2. Theoretical inferences and modeling, *Water Resour. Res.*, *51*, 2793–2806, doi:10.1002/2014WR016508.

Rango, A., and J. Martinec (1995), Revisiting the Degree-Day method for snowmelt computations, *Water Resour. Bull.*, *31*(4), 657–669, doi:10.1111/j.1752-1688.1995.tb03392.x.

Rinaldo, A., and A. Marani (1987), Basin scale-model of solute transport, *Water Resour. Res.*, *23*(11), 2107–2118, doi:10.1029/WR023i011p02107.

Rinaldo, A., and I. Rodriguez-Iturbe (1996), Geomorphological theory of the hydrological response, *Hydrol. Processes*, *10*(11), 803–829, doi:10.1002/(SICI)1099-1085(199606)10:6 < 803::AID-HYP373 > 3.0.CO;2-N.

Rinaldo, A., A. Marani, and A. Bellin (1989), On mass response functions, *Water Resour. Res.*, *25*(7), 1603–1617.

Rinaldo, A., K. J. Beven, E. Bertuzzo, L. Nicotina, J. Davies, A. Fiori, D. Russo, and G. Botter (2011), Catchment travel time distributions and water flow in soils, *Water Resour. Res.*, *47*, W07537, doi:10.1029/2011WR010478.

Rinaldo, A., P. Benettin, C. J. Harman, M. Hrachowitz, K. J. McGuire, Y. van der Velde, E. Bertuzzo, and G. Botter (2015), Storage selection functions: A coherent framework for quantifying how catchments store and release water and solutes, *Water Resour. Res.*, *51*, 4840–4847, doi:10.1002/2015WR017273.

Saccone, L., D. J. Conley, G. E. Likens, S. W. Bailey, D. C. Buso, and C. E. Johnson (2008), Factors that control the range and variability of amorphous silica in soils in the Hubbard Brook Experimental Forest, *Soil Sci. Soc. Am. J.*, *72*(6), 1637–1644, doi:10.2136/sssaj2007.0117.

Scanlon, T., J. Raffensperger, and G. Hornberger (2001), Modeling transport of dissolved silica in a forested headwater catchment: Implications for defining the hydrochemical response of observed flow pathways, *Water Resour. Res.*, *37*(4), 1071–1082, doi:10.1029/2000WR900278.

Seeger, S., and M. Weiler (2014), Reevaluation of transit time distributions, mean transit times and their relation to catchment topography, *Hydrol. Earth Syst. Sci.*, *18*(12), 4751–4771, doi:10.5194/hess-18-4751-2014.

Stelzer, R. S., and G. E. Likens (2006), Effects of sampling frequency on estimates of dissolved silica export by streams: The role of hydrological variability and concentration-discharge relationships, *Water Resour. Res.*, *42*, W07415, doi:10.1029/2005WR004615.

Stewart, M. K., U. Morgenstern, J. J. McDonnell, and L. Pfister (2012), The hidden streamflow challenge in catchment hydrology: A call to action for stream water transit time analysis, *Hydrol. Processes*, *26*(13), 2061–2066, doi:10.1002/hyp.9262.

Subbarao, G. V., O. Ito, W. L. Berry, and R. M. Wheeler (2003), Sodium a functional plant nutrient, *Crit. Rev. Plant Sci.*, *22*(5), 391–416, doi:10.1080/07352680390243495.

ter Braak, C. J. F., and J. A. Vrugt (2008), Differential evolution Markov chain with snooker updater and fewer chains, *Stat. Comput.*, *18*(4), 435–446, doi:10.1007/s11222-008-9104-9.

Tobin, C., B. Schaefli, L. Nicotina, S. Simoni, G. Barrenetxea, R. Smith, M. Parlange, and A. Rinaldo (2013), Improving the Degree-Day method for sub-daily melt simulations with physically-based diurnal variations, *Adv. Water Resour.*, *55*, 149–164, doi:10.1016/j.advwatres.2012.08.008.

van der Velde, Y., G. H. de Rooij, J. C. Rozemeijer, F. C. van Geer, and H. P. Broers (2010), Nitrate response of a lowland catchment: On the relation between stream concentration and travel time distribution dynamics, *Water Resour. Res.*, *46*, W11534, doi:10.1029/2010WR009105.

van der Velde, Y., P. J. J. F. Torfs, S. E. A. T. M. van der Zee, and R. Uijlenhoet (2012), Quantifying catchment-scale mixing and its effect on time-varying travel time distributions, *Water Resour. Res.*, *48*, W06536, doi:10.1029/2011WR011310.

van der Velde, Y., I. Heidbuchel, S. W. Lyon, L. Nyberg, A. Rodhe, K. Bishop, and P. A. Troch (2014), Consequences of mixing assumptions for time-variable travel time distributions, *Hydrol. Processes*, *29*(16), 3460–3474, doi:10.1002/hyp.10372.

Vrugt, J., C. T. Braak, C. Diks, B. Robinson, J. Hyman, and D. Higdon (2009), Accelerating Markov chain Monte Carlo simulation by differential evolution with self-adaptive randomized subspace sampling, *Int. J. Nonlinear Sci. Numer. Simul.*, *10*(3), 271–288, doi:10.1515/IJNSNS.2009.10.3.273.

Zimmer, M. A., S. W. Bailey, K. J. McGuire, and T. D. Bullen (2013), Fine scale variations of surface water chemistry in an ephemeral to perennial drainage network, *Hydrol. Processes*, *27*(24), 3438–3451, doi:10.1002/hyp.9449.